OPEN ACCESS
Fractals, Vol. 29, No. 2 (2021) 2140010 (16 pages)

DOI: 10.1142/S0218348X21400107

World Scientific
www.worldscientific.com

FRACTAL CHARACTERIZATION AND MECHANICAL BEHAVIOR OF PILE–SOIL INTERFACE SUBJECTED TO SULFURIC ACID

JIE XIAO,[*,¶] WENJUN QU,[†] HAIBO JIANG,[*,‖] LONG LI,[‡]
JUAN HUANG[*] and LIN CHEN[§]
[*]*School of Civil and Transportation Engineering*
Guangdong University of Technology, Guangzhou 510006, P. R. China
[†]*College of Civil Engineering, Tongji University*
Shanghai 200092, P. R. China
[‡]*Department of Civil and Environmental Engineering*
The Hong Kong Polytechnic University, Hong Kong, P. R. China
[§]*Shanghai Baoye Group Corp., Ltd., Shanghai 200941, P. R. China*
[¶]*xiaojie2017@gdut.edu.cn*
[‖]*hbjiang@gdut.edu.cn*

Received April 23, 2020
Accepted August 3, 2020
Published February 16, 2021

Abstract

This study aimed to investigate the different performance of pile–soil interfaces when the concrete was subjected to sulfuric acid corrosion. A series of large-scale direct shear tests were carried out to study the influence of sulfuric acid corrosion on the interface between soil and concrete pile. Concrete specimens immersed in sulfuric acid solution for different durations (0, 31, 93 and 154 days) were used to simulate the concrete pile surface roughness under sulfuric acid environment, which would be more realistic than the artificially roughened surfaces. Sand

[‖]Corresponding author.

was used to simulate the soil. Geometric models of concrete specimens attacked by sulfuric acid were captured using a 3D laser scanning technology, and fractal dimension was adopted to evaluate the surface characterization of concrete subjected to sulfuric acid. The shear stress–displacement curves of the interface between sand and corroded concrete were measured. The shear strength parameters and the Clough–Duncan hyperbolic model parameters were obtained. The relationship between friction angle and fractal dimension was established. The results of the tests showed that with the increase of the corrosion duration, the concrete surface became rougher, the fractal dimensions of concrete surface, the sand-corroded concrete interface friction angle, and the shear displacement at peak stress became larger. A nonlinear relationship was found between the fractal dimension and interface friction angle. The results could provide a reference to diagnose, evaluate, and analyze the interface behavior between sulfuric acid corroded concrete materials and soil.

Keywords: Sulfuric Acid; Fractal Dimension; Sand–Concrete Interface; Direct Shear Test; 3D Laser Scanning Technique.

1. INTRODUCTION

Many geotechnical engineering problems commonly involve the estimation of stresses transferred along the interface between soil and structure interfaces, such as pile foundations, retaining structures, slope protection, earth reinforcement, etc. It is essential to study the behavior of the interface between soil and structure materials for the comprehension of interaction mechanisms between them.[1–3] Many researchers have adopted direct shear apparatus, simple shear apparatus, and torsional shear apparatus to study the mechanical properties of the interface between soil and structure materials.[4] Direct shear apparatus has been the common choice for interface testing in research and application due to its wide availability, relatively simple test setup and sample preparation procedures.[5–9] As early as 1961, Potyondy[10] found that the interface shear resistance depended on various aspects such as construction materials type, soil type, surface roughness, normal stress, and moisture content. As one of the most significant influencing factors of the soil–structure interface,[11–13] the interface roughness has attracted the attention of many researchers. In order to study the interface property between soil and structure at different roughnesses, three issues need to be considered: how to produce rough surfaces, how to measure rough surfaces, and how to calculate roughness evaluation parameters.

First, most of the researchers adopted regular, man-made rough surfaces to simulate the interfacial roughness of actual piles. Hu *et al.*[2] and Wang *et al.*[14] grooved steel plates to manufacture different rough surfaces. Chu *et al.*[15] used cement grout plates with different waviness angles and the same width of the waviness "teeth" to produce different roughness. Chen *et al.*[16] employed a number of grooved trench with a semicircular cross-section and a diameter of 5 cm was laid out in parallel and regular on the concrete to obtain five different target roughness values. Taha *et al.*[17] used sand blasting and disc grinding to produce two different rough surfaces for concrete samples. Qian *et al.*[18] used ribbed concrete slabs with rib spacing of 125 mm (4 ribs), 170 mm (3 ribs) and 250 mm (2 ribs) to simulate the rib effect on the soil and helical pile interface resistance. Zhao *et al.*,[19] Zhang *et al.*[20] and Su *et al.*[21] respectively utilized concrete plates and steel plates formed by regular saw tooth to produce different rough surfaces. Han *et al.*[22] employed steel interfaces with four different levels of rusting to simulate the surface roughness of production steel piles more closely than artificially roughened surfaces. Sharma *et al.*[23] prepared two types of rough surfaces by gluing fine sand and medium sand particles on the smooth surface of mild steel. These previous studies have shown that the soil–structure interface mechanical properties are greatly influenced by the roughness. Although many useful conclusions have been obtained through regularly and artificially roughened surfaces in most previous studies, the irregular surface caused by specific engineering corrosion can more realistically simulate the surface roughness of the pile in a corrosive environment.

Second, roughness measurement methods can be classified as contact methods or non-contact methods, and roughness evaluation methods can be classified as qualitative methods or quantitative

methods. It is ideal to use a non-destructive testing method for roughness measurement and a quantitative method for roughness evaluation.[24] The first method was proposed by the International Institute for Concrete Repair (ICRI) to evaluate the surface roughness by comparing the visual inspection of the prepared surface with nine standard concrete surface profiles (CSP). This method was obviously fast and easy to perform, but it was a purely qualitative evaluation.[25] The simplest quantitative method named Sand Patch Test was inexpensive and convenient to perform. However, it was limited to horizontal surfaces, and the parameter was insensitive to micro-texture characteristics.[26] Then, the Mechanical Stylus was widely used to assess the surface roughness under laboratory conditions. However, this method has some disadvantages that the precision was affected by such factors as the dimensions, and movement speed of the probe and the surface may sustain damage during the measurement process.[27] In recent years, laser scanning technology had been developed in the fields of medicine, automotive, aerospace, historic building protection, civil engineering,[28,29] because it had the obvious advantages of high measuring accuracy, good portability, automatic reconstruction of 3D shapes, non-destruction and non-contaction to the detected object. In this paper, geometric models of the rough surface were captured using a 3D laser scanning technology.

Third, in terms of roughness evaluation methods, the value of surface roughness ($R_{\max}$) and the normalized roughness (R_n) were two frequently used roughness evaluation parameters in previous studies. $R_{\max}$ was evaluated based on the maximum height vertical span between the highest peak and the lowest valley along a surface profile over a gauge length on the surface,[17,19,30] while R_n was defined as the ratio of $R_{\max}$ to the average grain diameter (D_{50}).[2,13,21,31] Compared with the statistical methods that strongly depended on the resolution and the sampling range of the measurement instrument applied, the use of fractal dimensions to characterize the surface roughness had obvious advantages. For example, the fractal dimensions could be determined independently from the resolution and sampling range of the roughness measurement instrument.[32] So far, many studies have confirmed that the fractal dimension was capable for the estimation of steel corrosion resistance characterization,[33,34] pore evolution in cementitious materials,[35] and development of fracture in rock surface.[36,37] In this paper, the fractal dimension was adopted to evaluate the surface roughness.

Due to the alkaline nature of concrete, deterioration occurred when concrete structures were exposed to acidic environments.[38–41] Sulfuric acid was a most frequently encountered acid environment in engineering practice, which mainly generated from the oxidation of sulfur compounds (e.g. sulfur dioxide,[42,43] pyrite[44]) or bacterial activities.[45,46] In the complex process of sulfuric acid attacking the concrete piles, confining pressure, and the rough concrete surface were the two main factors that may affect the skin friction between concrete and soil. It was observed in previous studies that friction force was directly proportional to normal forces. So confining pressure due to expansive reactions products produced by the chemical reaction of concrete and sulfuric acid (mainly gypsum[47–49]) should had a positive effect on skin friction. However, it was not clear whether the effect of sulfuric acid corrosion on the skin friction between concrete pile and soil negative or positive.[50]

In this study, the concrete surface was produced through sulfuric acid corrosion, and laser scanning technology and fractal geometry theory were respectively employed to measure the rough surface and calculate roughness evaluation parameters. This study aimed to investigate the different performance of pile–soil interfaces when the concrete was subjected to sulfuric acid corrosion, which was rarely reported in previous research. A series of large scale direct shear tests were carried out to study the influence of sulfuric acid corrosion on the interface between sand and concrete. Concrete specimens immersed in sulfuric acid solution for different days were used to simulate the pile under sulfuric acid environment. Although the pile foundation accident caused by sulfuric acid was rarely reported due to the large safety factor,[51] the influence of concrete piles degradation caused by sulfuric acid attack on skin friction at the pile–soil interface still needs to be investigated. The results in this study could be a reference to diagnose, evaluate, and analyze the interface behavior between sulfuric acid corroded concrete materials and soil.

2. TEST PROGRAM

2.1. Large Direct Shear Test Apparatus

The large direct shear test apparatus employed in this paper were designed and manufactured in

Table 1 Main Technical Parameters of the Large Direct Shear Test Apparatus.

Shear Box Net Size/mm	Maximum Load/kN		Maximum Displacement/mm		Shear Rate/ (mm/min)	Accuracy in Measurement/%
	Normal Direction	Tangential Direction	Normal Direction	Tangential Direction		
600 × 400 × 200	200	200	50	150	0.1–50	0.5

Tongji University, China, which is the same as the apparatus in Ref. 18. The apparatus consisted of three major parts: measurement and control unit, hydraulic servo unit, loading unit. Its main technical parameters were listed in Table 1. The dimensions of the upper shear box and lower shear box were both 600 mm on the shear direction, 400 mm in width and 100 mm in depth. The front walls in the middle of the upper and lower shear boxes near the contact surface were made of Plexiglas plate, allowing to observe the shear deformation of soil layers. Horizontal and vertical loads were applied via hydraulic actuators. Horizontal and vertical displacements were monitored by linear variable differential transformers (LVDTs). These loads and displacements were logged at the interval of 0.4 s using an automatic data logger system connected to a computer. On the large direct shear test apparatus, constant force control, constant force rate control, constant displacement control, and constant displacement rate control can be realized in vertical and horizontal directions. The lower shear box was placed with concrete, and the upper shear box was filled with soil. The upper shear box, where a normal load was applied on to the specimen, was fastened, and the lower shear box was able to move to simulate the movement of piles in the soil.[52]

2.2. Concrete Specimen

In this investigation, raw materials of concrete came from Sanhe Pipe Pile Corporation at Suzhou in China. Local Portland cement (P · II 52.5R) with a 28d compressive strength of 55.3 MPa was used. Coarse aggregate with a maximum nominal size of 25 mm and water absorption of 0.92% and fine aggregates with a fineness modulus of 2.61 and water absorption of 1.79% was used for concrete specimens. The water to cement ratio was 0.45 (by weight), and the mixture proportions per cubic meter of concrete were 205 kg water, 456 kg cement, 516 kg fine aggregates, and 1149 kg coarse aggregates. Four 600 mm × 400 mm × 50 mm (length × width × height) concrete plates were cast as the structure materials. After 28 days of curing, concrete plates were fully soaked in a plastic vessel containing an aggressive sulfuric acid solution. In order to accelerate the corrosion process, the pH value around 0.95 was used in this study according to the previous studies.[41,53] The rough surfaces of concrete plates were produced by complete immersion in a sulfuric acid solution of pH ≈ 0.95 for 0, 31, 93, 154 days (the actual immersing days). A portable pH meter (accuracy 0.01) was used to measure the pH of solutions during the testing period of nearly five months. It was kept in the range of 0.93 to 0.97 by daily adjusting the pH value using concentrated sulfuric acid. The solution was gently stirred after adding the concentrated sulfuric acid every day in order to reduce differential concentrations of the acid within the solution vessel. The sulfuric acid solution was refreshed every month.

2.3. Soil Materials

As the goal of this research was to investigate the influence of the concrete piles surface roughness caused by sulfuric acid attack on the interface properties between corroded concrete and soil. Soil samples could have introduced other effects, whose influence on the interface properties between corroded concrete and soil would have been difficult

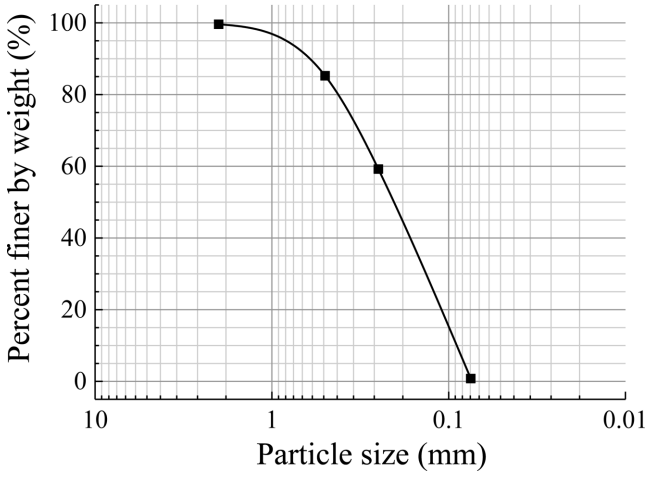

Fig. 1 Particle size distribution curves of the sand.

Table 2 Basic Material Properties of the Sand.

Specific Gravity	Water Content/ %	Density/g/cm^3		Void Ratio		Coefficient of Uniformity C_u	Coefficient of Curvature C_c
		ρ_{max}	ρ_{min}	e_{max}	e_{max}		
2.58	0.04	1.726	1.453	0.776	0.495	2.78	1.00

to be analyzed separately. The sand was selected to be the soil samples in this experiment because of its relatively uniform and stable properties. The particle size distribution curve of the sand was shown in Fig. 1, and the basic material properties of the sand were listed in Table 2.

2.4. Test Procedure

2.4.1. *Corrosion surface topography obtained by laser scanning technology*

In this study, the surface topographies of all corroded concrete specimens after cleaning and drying were measured using a handheld 3D laser scanner T-SCAN CS produced by German Steinbichler Optoelectronics Technology Co., Ltd. Based on triangulation techniques and light sweeping method, the 3D coordinates of each point on the specimen surface could be obtained. Afterwards, the 3D coordinates of each point (i.e. point cloud) on the surface of the corroded concrete were acquired, which will be further processed with the software MATLAB 2013.

The cubic covering method proposed by Zhou and Xie[37] was adopted to calculate the corroded surface fractal dimension. A brief description of the calculation principle of the surface fractal dimension was as follows: There was a regular square grid ABCD on the plane XOY, as shown in Fig. 2. In each grid with side length δ, four intersection points corresponded to four heights of a rough surface: $h(i,j)$, $h(i,j+1)$, $h(i+1,j)$ and $h(i+1,j+1)$ (where $1 \le i \le m-1$, $1 \le j \le n-1$, m and n were the total number of sampling points on a rough surface in the x-axis and y-axis directions, respectively). If a cube with a side length δ was used to cover the rough surface, the maximum difference among $h(i,j)$, $h(i,j+1)$, $h(i+1,j)$ and $h(i+1,j+1)$ would determine the number $N_{i,j}$ of cubes required to cover the irregular surface area within the scale δ:

$$N_{i,j} = \mathrm{INT}\left\{\frac{1}{\delta}[\max(h(i,j), h(i,j+1), \times h(i+1,j), h(i+1,j+1)) - \min(h(i,j), h(i,j+1), h(i+1,j), \times h(i+1,j+1))] + 1\right\}, \quad (1)$$

where INT denoted the integrating function. When the cube side length was δ, the total number of cubes covered the entire rough surface that can be expressed as

$$N(\delta) = \sum_{i,j=1}^{n-1} N_{i,j}. \quad (2)$$

By changing the side length δ of the cubes, the process was repeated to calculate the different number of cubes $N(\delta)$ and was required to completely cover the rough surface. Obviously, a smaller δ will yield a larger $N(\delta)$.

According to the fractal theory, if the relation between the total number of cubes $N(\delta)$ and the cube side length δ obeyed the following functional relationship, the rough surface exhibited fractal characteristics

$$N(\delta) \sim \delta^{-D}, \quad (3)$$

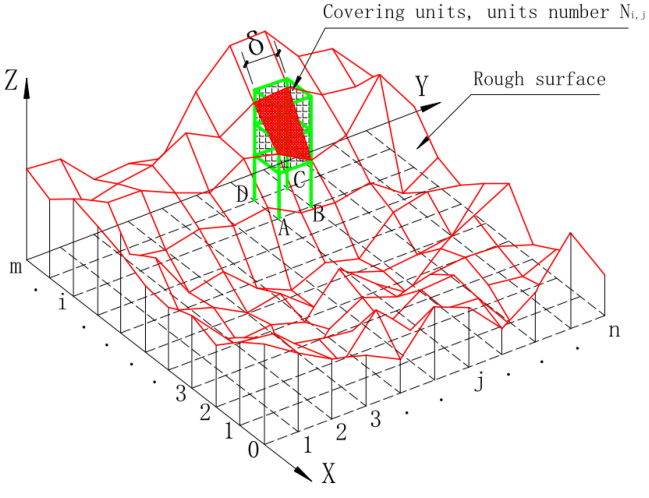

Fig. 2 Schematic view of cubic covering method.

where D was the fractal dimension of the rough surface.

2.4.2. *Interface direct shear test*

The concrete plate was installed in the lower shear box, and the upper shear box was used to place test sand. The upper shear box filled with sand was immobile, while the lower box was driven to move by a tangential force applied via a hydraulic actuator. The soil pressure around the concrete pile was simulated by the normal force of the direct shear apparatus, and the vertical load on the concrete pile was simulated by the tangential force of the direct shear equipment, as illustrated in Fig. 3. In order to reduce weight and easy to facilitate manually, the thickness of concrete specimen was chosen to be 50 mm instead of 100 mm that was the depth of the lower shear box, and steel pad was placed underneath the concrete specimen for adjusting the position of the interface between concrete and sand. It was a very critical issue to determine the location of the interface between corroded concrete and sand, which was determined based on the following reason in this experiment. The roughness of the side of the concrete pile was supposed to be in a regular sawtooth shape after the concrete pile was corroded, as shown in Fig. 3a. Because the shear strength of concrete was much larger than soil, the shear strength of the 2-2 plane in Fig. 3a will be higher than that of a 1-1 plane. For this reason, the 1-1 plane was selected as the shearing interface, so the concrete specimen placement in this experiment was shown in Fig. 3b.

A given mass (30 kg) of the sand was weighed and manually compacted into three layers toward a controlled volume in the upper shear box in order to achieve the target relative density. During shearing, the normal and tangential forces at the interface were measured by load cells, and the vertical and horizontal displacements at the interface were monitored by a system of four linear variable displacement transducers (LVDTs). All specimens were conducted under normal stresses of 50, 100, 150 and 200 kPa, which were commonly found in geotechnical engineering applications. Shear stress was applied on the lower shear box until an initial normal stress 200 kPa for 20 min and the normal deformation had become stable. A data acquisition system connected to a computer constantly monitored and recorded the readings from the load cells and LVDTs. A shear displacement rate of 2.0 mm/min was used in this study, and the shearing process was terminated when the tangential displacement reached 35 mm since the wall thickness of the shear box was 40 mm. In addition to the shear test of the interface between the concrete specimens and the sand, the shear behavior of the sand itself was tested according to the above shear test procedure, except for the following differences: a given mass (30 kg) of the sand was weighed and manually compacted into three layers toward a controlled volume in the lower shear box. Then, another given mass (30 kg) of the sand was weighed and manually

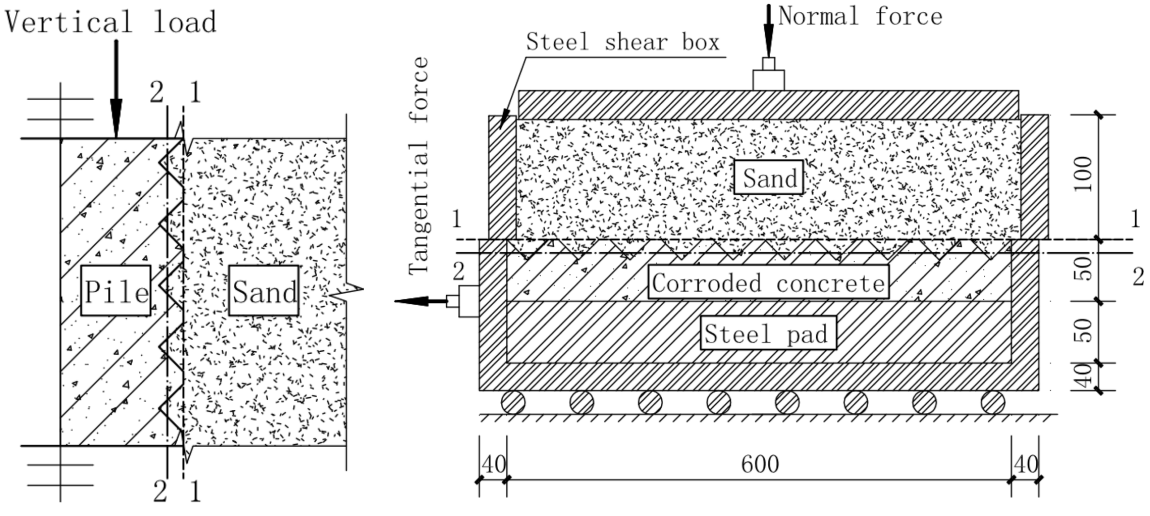

(a) Corroded pile and soil **(b)** Corroded concrete specimen and soil in shear box

Fig. 3 Illustration of the selection of the location of the interface between corroded concrete and sand.

compacted into three layers toward a controlled volume in the upper shear box.

3. TEST RESULTS AND ANALYSIS

3.1. Visual Inspection

Photographs of concrete specimens were taken after immersion in the sulfuric acid over regular time periods (0, 31, 93 and 154 days) to record changes in surface appearance, as illustrated in Fig. 4. The corrosion process was clearly shown in the photographs: the uncorroded surface was flat and smooth after demolding. After 31 days of immersion, the dissolution effect of sulfuric acid caused the exposure of sand grains and the residual of white corrosion products (mainly gypsum). From 31 days immersion to 154 days immersion, the cement paste started to dissolve layer by layer from the surface to the inside, with the gradual shedding of smaller aggregates and the gradual exposure of larger aggregates.

3.2. Calculation Results of Fractal Dimension

The MATLAB program was written to implement the cubic covering method mentioned in Sec. 2.4.1 with the coordinate data file of the corroded surface point obtained by laser scanning technology. In Matlab 2013, data processing and reconstruction based on the coordinate data files of concrete specimens corroded for 0, 31, 93 and 154 days were performed, as presented in Fig. 5. Nine different grid numbers were selected for the four concrete specimens to produce nine kinds of different side lengths cubes: 75×50, 150×100, 300×200, 600×400, 900×600, 1200×800, 1500×1000, 2100×1400 and 3000×2000. Then, in these nine cases, the number of the square boxes $N(\delta)$ required to completely cover the surface by cubes with side length δ were respectively obtained. The fractal dimension could be calculated from the relationship between $N(\delta)$ and δ as the above-mentioned Eq. (3). Usually, the value of fractal dimension can be estimated from the slope of dual logarithmic coordinate graphs of $\ln(N(\delta))$ against $\ln(\delta)$, as shown in Fig. 6. After

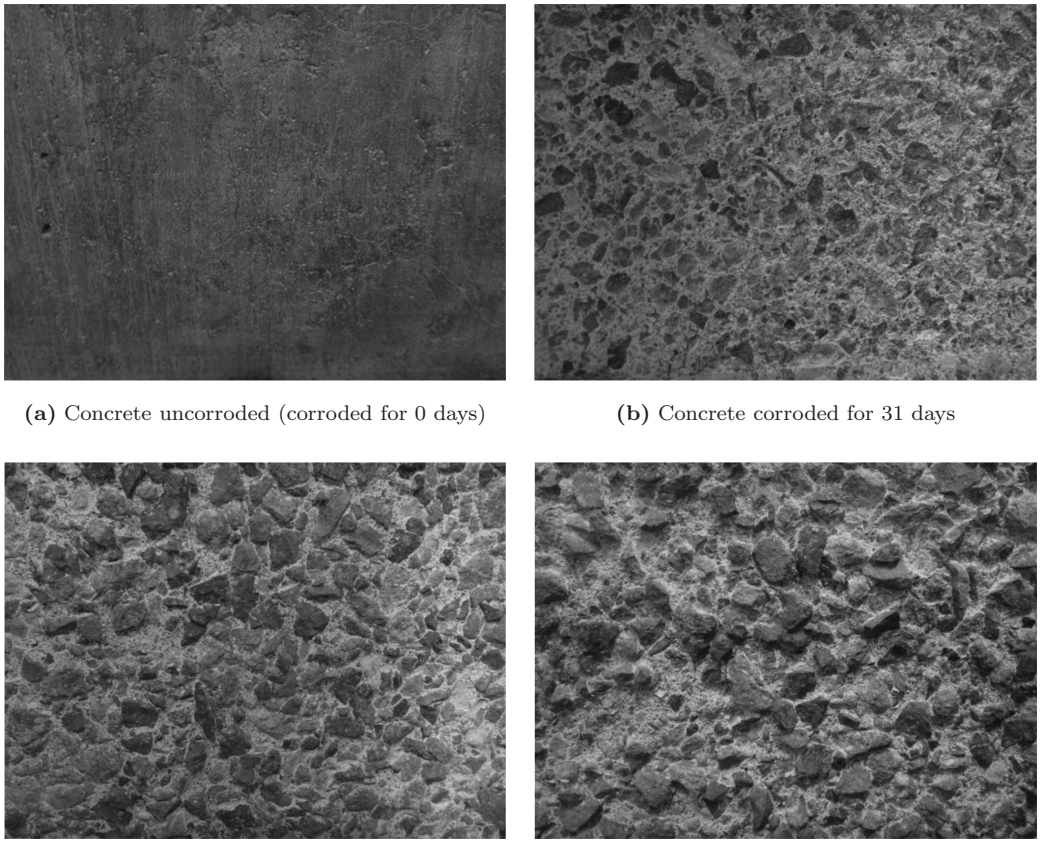

(a) Concrete uncorroded (corroded for 0 days)

(b) Concrete corroded for 31 days

(c) Concrete corroded for 93 days

(d) Concrete corroded for 154 days

Fig. 4 Photograph of concrete specimens corroded for 0, 31, 93 and 154 days.

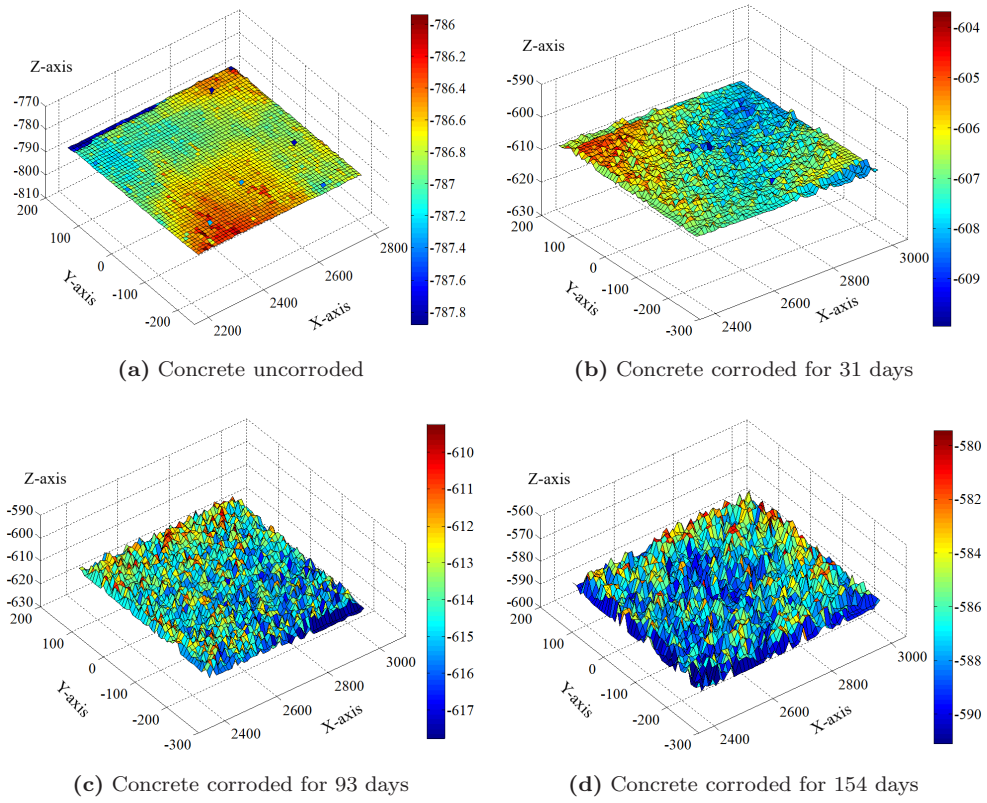

(a) Concrete uncorroded **(b)** Concrete corroded for 31 days

(c) Concrete corroded for 93 days **(d)** Concrete corroded for 154 days

Fig. 5 Reconstruction of the concrete specimens surfaces corroded for 0, 31, 93 and 154 days in Matlab.

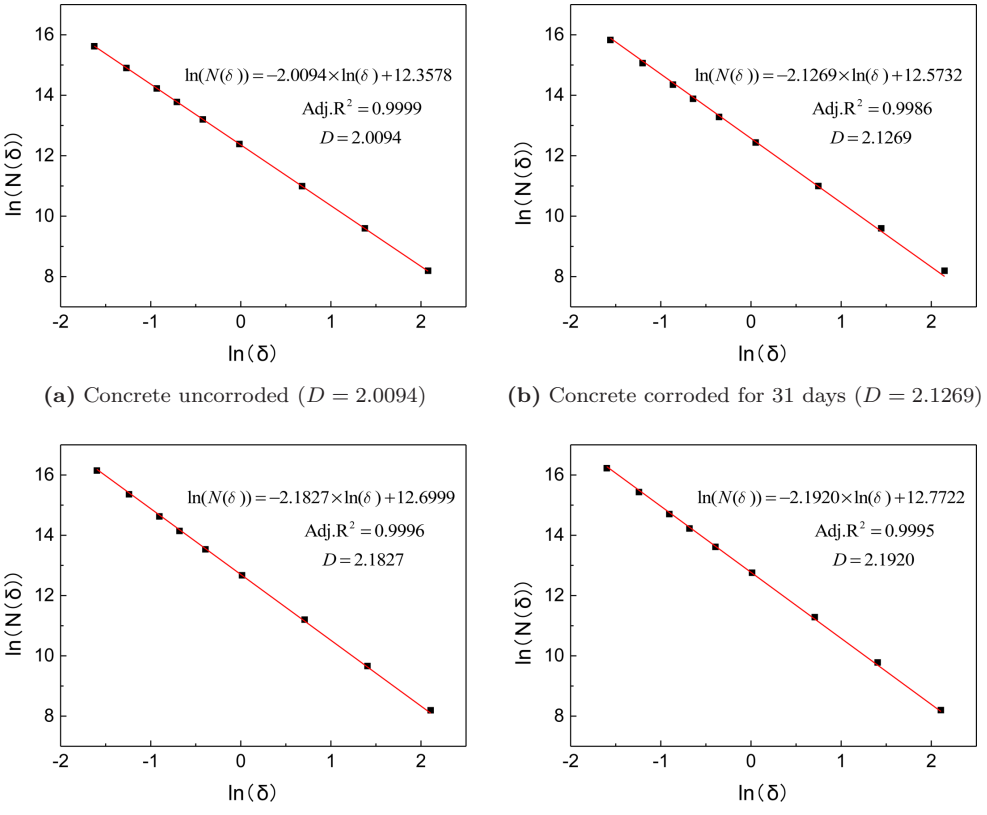

(a) Concrete uncorroded ($D = 2.0094$) **(b)** Concrete corroded for 31 days ($D = 2.1269$)

(c) Concrete corroded for 93 days ($D = 2.1827$) **(d)** Concrete corroded for 154 days ($D = 2.1920$)

Fig. 6 Dual logarithmic coordinate graphs of concrete specimens corroded for 0, 31, 93 and 154 days to calculate fractal dimensions.

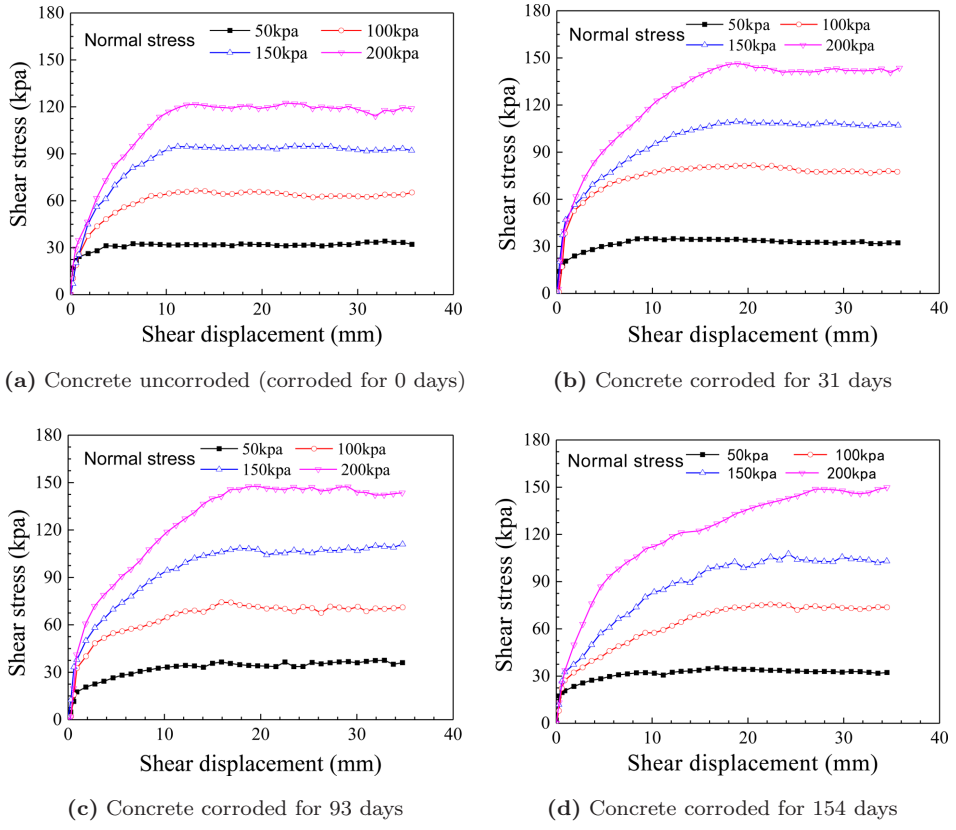

(a) Concrete uncorroded (corroded for 0 days)

(b) Concrete corroded for 31 days

(c) Concrete corroded for 93 days

(d) Concrete corroded for 154 days

Fig. 7 Curves of the interface shear stress–displacement between sand and concrete specimens corroded different days.

calculation, the fractal dimensions of concrete specimens corroded for 0, 31, 93 and 154 days were 2.0094, 2.1269, 2.1827 and 2.1920, respectively. The initial fractal dimension of the uncorroded concrete surface was almost equal to 2.00, which meant that the concrete specimen surface after demolding was almost a two-dimensional smooth plane. As the corrosion time increased, the dissolution of the cement paste and the exposure of the aggregate caused the surface to become rougher, so the fractal dimension characterized the surface roughness increased with the increase of the corrosion time.

3.3. Interface Direct Shear Test Results

The shear stress–displacement curves of the interface between sand and concrete specimens corroded for 0, 31, 93 and 154 days were shown in Figs. 7a–7d. From these curves, it can be seen that the shear stress initially increased linearly with the gradual increase of the shear displacement, and the shear modulus of the interface was constant and relatively high at the initial stage. The curves tended to deviate from linearity with a continuous increase of the shear displacement, which indicated that the interface yielded. Thereafter, the shear stress hardly increased with the further increase of the shear displacement. There was no obvious peak in the curves of the interface shear stress–displacement between sand and concrete specimens after corroded for different days. Therefore, it was reasonable to take the yielding stress of the interface as the shear strength. Shear stress and shear displacement of the interface between sand and concrete specimens

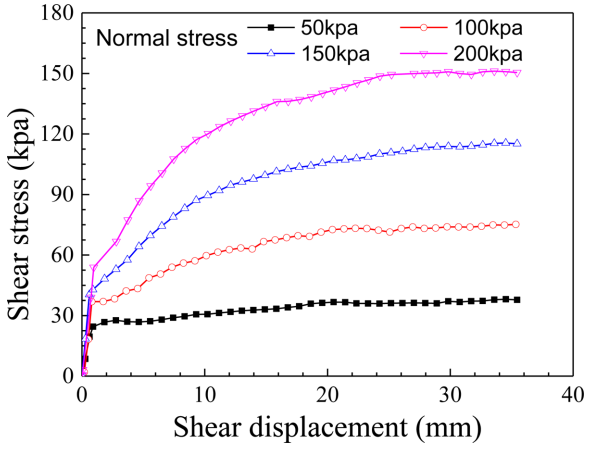

Fig. 8 Interface shear stress–displacement curves of sand itself.

Table 3 Direct Interface Shear Test Results and Fitted Parameters of Test Data.

Test Plan	Corrosion Time/Days	Normal Stress σ/kPa	Direct Interface Shear Test Results					Fitting Parameters		
			Peak Stress τ_f/kPa	Displacement at Peak Stress ω_f/mm	Cohesive c/kPa	Friction Angle $\varphi/^\circ$	Adj $\cdot R^2$	a	b	Adj $\cdot R^2$
Direct shear test for sand and concrete specimens subjected to sulfuric acid for different days	0	50	32.79	6.57	3.39	30.87	0.996	0.0197	0.0303	0.997
		100	66.88	13.25				0.0170	0.0149	0.996
		150	96.15	11.97				0.0126	0.0103	0.997
		200	122.58	12.82				0.0121	0.0080	0.994
	31	50	35.33	8.79	1.82	36.02	0.990	0.0346	0.0282	0.987
		100	82.07	20.05				0.0273	0.0118	0.990
		150	110.16	18.63				0.0198	0.0088	0.994
		200	147.10	18.78				0.0166	0.0065	0.996
	93	50	37.28	15.30	0.155	36.64	0.999	0.0463	0.0262	0.996
		100	75.36	16.78				0.0258	0.0131	0.996
		150	110.25	18.30				0.0208	0.0086	0.997
		200	149.61	19.17				0.0187	0.0063	0.993
	154	50	35.34	16.90	0.106	37.00	0.996	0.0401	0.0282	0.993
		100	76.58	21.88				0.0361	0.0121	0.991
		150	107.97	22.98				0.0323	0.0084	0.992
		200	150.46	34.54				0.0272	0.0059	0.997
Direct shear test for the sand itself		50	36.98	20.04	0.055	37.61	0.998	0.0626	0.0250	0.996
		100	73.77	22.20				0.0438	0.0121	0.998
		150	115.87	34.03				0.0349	0.0077	0.999
		200	151.36	33.48				0.0231	0.0059	0.997

corroded for different days showed a good elasto-plastic relationship, which can be described by the hyperbolic model. For the sand itself, shear stress–displacement curves of the interface between sand and sand were obtained by the same test procedure as that between sand and concrete, as illustrated in Fig. 8. The test results were listed in Table 3. The shear strength increases with the increase of normal stress as shown in Figs. 10 and 11, and the relationship between shear strength and normal stress will be explored in the next paragraph.

Figure 9 illustrated the shear strengths under different normal stresses for interfaces of sand-corroded concrete for different days and the sand itself. The curves indicated that the shear strength increased linearly with regularly increasing normal stress and proved that the shear behavior of the sand-corroded concrete interface obeyed the Mohr–Coulomb criterion, as shown in Eq. (4). Based on this criterion, the shear strength parameters for the Mohr–Coulomb failure law (i.e. the cohesive and friction angle) can be obtained by linear regressed from the test data in Fig. 8 using the least-squares method, and the parameters were listed in Table 3.

$$\tau_f = \sigma \tan \varphi + c, \tag{4}$$

where τ_f was the shear strength (peak shear stress), kPa; σ was the normal stress, kPa; φ was the friction angle; c was the cohesive, kPa.

It can be found from Fig. 9 that the interface friction angle increased with the increase of the corrosion days, and the internal friction angle of interface for the sand itself was higher than the friction angle of sand-corroded concrete interface. This indicated that the rougher interfaces still exhibit weaker shearing resistance than the sand itself, but stronger shearing resistance than the smooth interface. The reason may be that failure planes exist in the sand instead of on the concrete surface.

It was well known that the bearing capacity of a pile foundation consists of two parts: the pile-end bearing and the pile shaft friction. During the loading process of a pile foundation, the shaft friction was mobilized first, whereas the end-bearing resistance was only mobilized after the pile shaft friction reaches its limiting value. Therefore, it was worth paying attention to the displacement when the pile shaft friction reached its peak value. In this paper, the shear displacement at peak stress was extracted from the shear stress–displacement curves of the concrete–sand interface. The related experimental data results were listed in Table 3, and the curves of shear displacement at peak stress with corrosion days were presented in Fig. 10. It can be found from Fig. 10, the shear displacement at peak stress generally increased with the increase of the corrosion days. This could imply that greater pile displacement may be required to take advantage of the higher resistance with concrete subjected to more severe corrosion.

It was very important to establish accurate models to the behavior of soil–structure interfaces in order to obtain realistic solutions to many soil–structure interaction problems. There were many models to simulate the behavior of soil and structure interface, such as the rigid plastic model,[54] the elastic-plastic model,[55] and the Clough–Duncan hyperbolic model. Among them, the hyperbolic model of shear stress and shear displacement proposed by Clough and Duncan had been widely

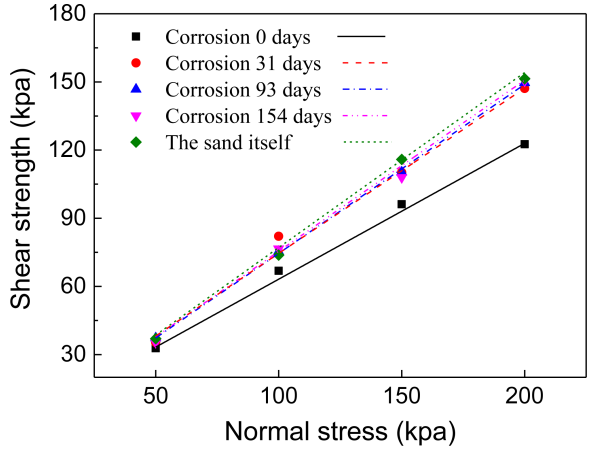

Fig. 9 The shear strengths under different normal stresses for interfaces of sand-corroded concrete for different days and sand itself.

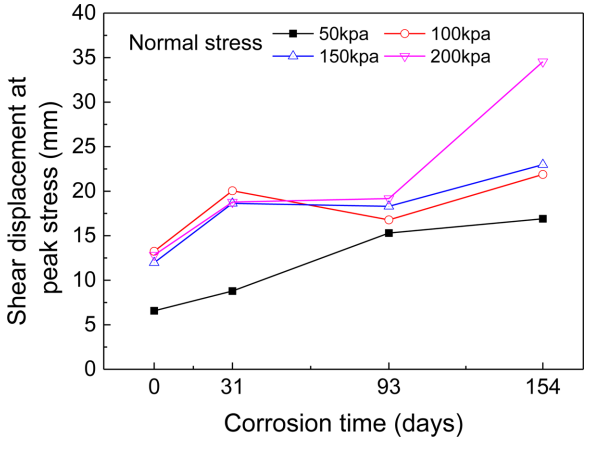

Fig. 10 Curves of shear displacement at peak stress with corrosion days.

used due to its simple formula form, easy parameters determination, and clear parameters physical meaning. The Clough–Duncan hyperbolic model expressed the shear stress and shear displacement curve of the interface by the following formula:

$$\tau = \frac{\omega}{a + b\omega}, \tag{5}$$

where τ was shear stress on the interface, ω was the shear displacement between sand and corroded concrete, a and b were fitted parameters using the shear stress and shear displacement curve obtained from shear tests. When the shear displacement ω of interface approached infinitely, the shear stress of interface approached a constant τ_f called ultimate shear stress value. When the shear displacement ω of interface approached zero, the ratio of shear stress to shear displacement approached the initial shear stiffness represented by the symbol k_{s0}. So, as illustrated in Eq. (6), the physical meaning of the fitted parameters a and b was the reciprocal of the initial shear stiffness and the ultimate shear stress value, respectively. The fitted results of parameters (a and b) for the hyperbolic contact model were obtained through shear stress and shear displacement curves of interface between sand and corroded concrete with different corrosion days. The fitted results of parameters (a and b) were listed in Table 3. For simplicity, a corroded concrete for 93 days was used as an example to illustrate the comparison of tested and modeled shear stress and shear displacement curves, as shown in Fig. 11. The comparison showed that the numerical model fits very well with the experimental data.

$$\begin{cases} \lim\limits_{\omega\to\infty} \tau = \lim\limits_{\omega\to\infty} \dfrac{\omega}{a + b\omega} = \dfrac{1}{b} = \tau_f \\ \lim\limits_{\omega\to 0} \dfrac{\tau}{\omega} = \lim\limits_{\omega\to 0} \dfrac{1}{a + b\omega} = \dfrac{1}{a} = k_{s0}. \end{cases} \tag{6}$$

3.4. Correlation Between Fractal Dimension and Interface Shear Strength

For sand and concrete interface, the interface friction angle played a decisive role in the shear strength, and the cohesion at the interface can be ignored in this study. Therefore, we explored the effect of roughness on the shear properties of the interface between sand and corroded concrete by exploring the relationship between friction angle and fractal dimension. A nonlinear relationship was found between the fractal dimension and interface friction angle. The interface friction angle increased faster in the early stages, but the growth rate gradually decreased in the later stages and tended to be stable, as shown in Fig. 12 and Eq. (7). The fitted result of $\mathrm{Adj} \cdot R^2$ is close to 1, which indicated, to a certain extent, the fitting formula fits the four test points in this paper well.

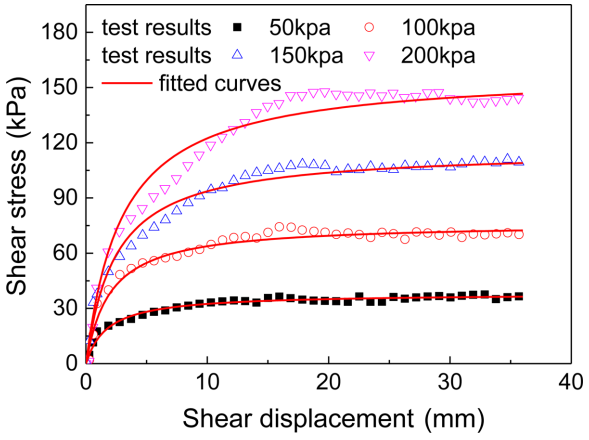

Fig. 11 The comparison of tested and modeled shear stress and shear displacement curves for concrete corroded for 93 days.

$$\varphi = 40.6 \times (D - 2)^{0.0581}, \tag{7}$$

where φ was the interface friction angle, and D represented the fractal dimension of the corroded concrete surface. The main reason for the rapid increase of interface friction angle in the early corrosion stages was that as the dissolution of cement paste, the gradual exposure of fine and coarse aggregate made the concrete surface rough from an initially smooth surface. During the later corrosion stages, a balance was formed that the gradual loss of the aggregate would decrease the surface roughness,

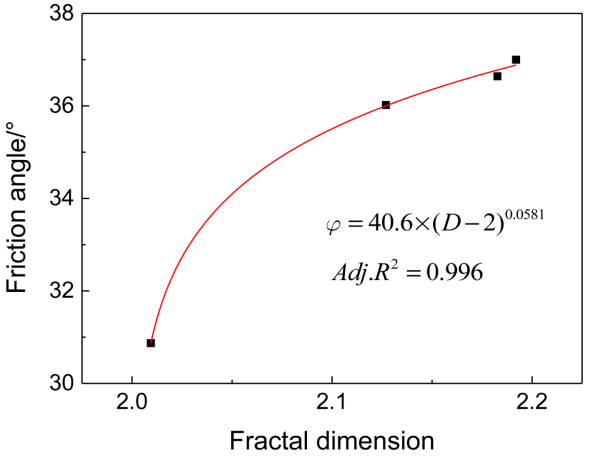

Fig. 12 Curves of fractal dimension and interface friction angle.

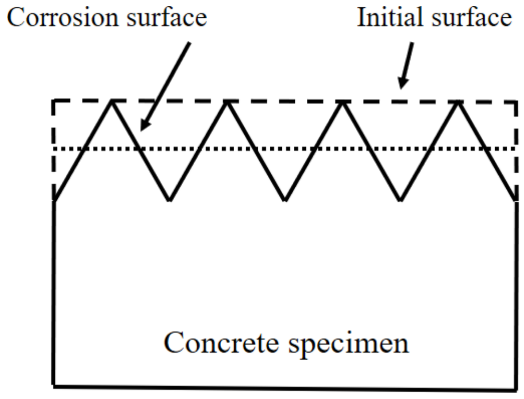

(a) During the early corrosion stages

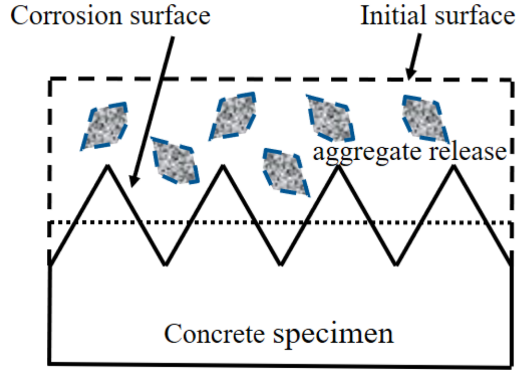

(b) During the later corrosion stages

Fig. 13 Analysis of the causes of surface roughness changes at different stages.

but the new exposure of aggregate due to cement paste dissolution would increase the surface roughness, which caused the roughness to become stable, as shown in Fig. 13.

Patton[56] established a bilinear failure criterion and found that the shear behavior of the joints was different depending on the magnitude of the normal stress applied through a series of direct shear tests on specimens with regular saw-teeth artificial joint. After the shear test in this paper, it was found that the aggregates on the concrete surface corroded by sulfuric acid were not sheared off due to shear, so the failure mechanism may be governed by the sliding overriding the asperities,[57] Patton used Eq. (8) to estimate the shear strength of irregular surfaces

$$\tau_f = \sigma \tan(\varphi + i) + c. \tag{8}$$

If the interface plane was flat, its shear strength was calculated by Mohr–Coulomb failure law as Eq. (4), where φ was friction angle, c was cohesion, τ_f was shear strength and σ was normal stress. If the interface plane was a regular saw-teeth interface with an undulation angle i, its shear strength was calculated

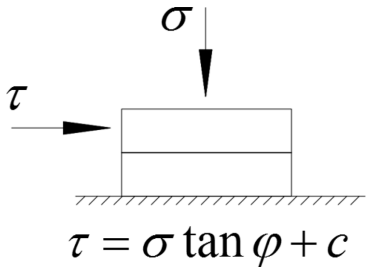

(a) Diagram of a flat interface

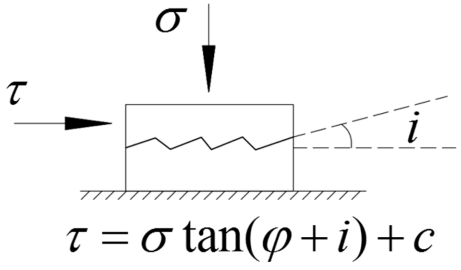

(b) Diagram of a regular saw–teeth interface

Fig. 14 Schematic diagram of regular saw–teeth interface increase friction angle.

as Eq. (8), as presented in Fig. 14. It could be seen that the interface friction angle of a regular saw-teeth interface with an undulation angle i would increase. In this test, the uncorroded concrete surface was equivalent to a smooth and flat surface, but due to the dissolution of the cement paste, the loss of fine aggregates and the exposure of coarse aggregate, the acid-corroded concrete surface exhibited an irregular jagged shape surface. With the increase of the corrosion time, the cement paste dissolution and the loss of fine aggregates would gradually increase the corrosion depth, and the exposure of coarse aggregate would gradually become sharper, which would increase the friction angle. Therefore, the acid corrosion had a great influence on the interface friction angle between sand and concrete.

4. CONCLUSIONS

(1) The results indicated that the concrete sulfuric acid corroded surfaces exhibited fractal characteristics. The fractal dimensions of the rough surfaces of concrete subjected to sulfuric acid increased with the increase of the corrosion time.

(2) Shear stress and shear displacement between sand and corroded concrete showed a good elastoplastic relationship, which can be described by the Clough–Duncan hyperbolic model. The relationship between shear strength

and normal stress of interface obeyed the Mohr–Coulomb criterion. The Mohr–Coulomb failure envelope of the corroded interfaces lies below the failure envelope of the sand.

(3) The shear displacement at peak stress increases with the increase of the corrosion days. This implied that greater pile displacement might be required to take advantage of the higher resistance with concrete subjected to more severe corrosion.

(4) With the increase of the corrosion days, the concrete surface became rougher, the interface friction angle increased and the shear strength increased. A nonlinear relationship was found between the fractal dimension and interface friction angle. The interface friction angle increased faster in the early stages, but the growth rate gradually decreased in the later stages and tended to be stable.

ACKNOWLEDGMENTS

The authors are appreciated for the financial support provided by the National Natural Science Foundation of China with No. 51808133, and the National Natural Science Foundation of China with Grant No. 51778150, and the National Natural Science Foundation of China with Grant No. 51678430.

REFERENCES

1. P. Yang, S. Xue, L. Song and M. Duan, Interface shear characteristics of dredger fill and concrete using large size direct shear test, *Int. J. Geo-Eng.* **9**(1) (2018) 15.
2. L. Hu and J. Pu, Testing and modeling of soil-structure interface, *J. Geotech. Geoenviron. Eng.* **130**(8) (2004) 851–860.
3. Z. M. Chen, L. J. Li and Z. Xiong, Investigation on the interfacial behavior between the rubber-cement matrix of the rubberized concrete, *J. Clean Prod.* **209** (2019) 1354–1364.
4. M. A. Hossain and J. Yin, Behavior of a pressure-grouted soil-cement interface in direct shear tests, *Int. J. Geomech.* **14**(1) (2014) 101–109.
5. J. E. Gomez, G. M. Fiz, R. M. Ebeling and J. E. Dove, Sand-to-concrete interface response to complex load paths in a large displacement shear box, *Geotech. Test. J.* **31**(4) (2008) 358–369.
6. G. W. Clough and J. M. Duncan, Finite element analyses of retaining wall behavior, *ASCE J. Soil Mech. Found. Div.* **97**(12) (1971) 1657–1673.
7. C. S. Desai, C. E. Drumm and M. M. Zaman, Cyclic testing and modeling of interfaces, *ASCE J. Geotech. Eng.* **111**(6) (1985) 793–815.
8. E. Evgin and K. Fakharian, Effect of stress paths on the behavior of sand-steel interfaces, *Can. Geotech. J.* **33**(6) (1996) 853–865.
9. Y. Wu, C. Zhao, C. Zhao, Y. Wang and Y. Fei, Effect of grout conditions on the mechanical behaviors of unloading sand-concrete interface for reinforcing bored pile foundation, *Constr. Build. Mater.* **243** (2020) 118218.
10. J. G. Potyondy, Skin friction between various soils and construction materials, *Geotechnique* **11**(4) (1961) 339–353.
11. M. Feligha, F. Hammoud, M. Belachia and M. S. Nouaouria, Experimental investigation of frictional behavior between cohesive soils and solid materials using direct shear apparatus, *Geotech. Geol. Eng.* **34**(2) (2016) 567–578.
12. M. Uesugi and H. Kishida, Influential factors of friction between steel and dry sands, *Soils Found.* **26**(2) (1986) 33–46.
13. M. Uesugi and H. Kishida, Frictional resistance at yield between dry sand and mild steel, *Soils Found.* **26**(4) (1986) 139–149.
14. X. Wang, X. Z. Wang, C. Q. Zhu and Q. S. Meng, Shear tests of interfaces between calcareous sand and steel, *Mar. Geores. Geotechnol.* **37**(9) (2019) 1095–1104.
15. L.-M. Chu and J. Yin, Study on soil–cement grout interface shear strength of soil nailing by direct shear box testing method, *Geomech. Geoeng.* **1**(4) (2006) 259–273.
16. X. B. Chen, J. S. Zhang, Y. J. Xiao and J. Li, Effect of roughness on shear behavior of red clay — Concrete interface in large-scale direct shear tests, *Can. Geotech. J.* **52**(8) (2015) 1122–1135.
17. A. Taha and M. Fall, Shear behavior of sensitive marine clay-concrete interfaces, *J. Geotech. Geoenviron. Eng.* **139**(4) (2013) 644–650.
18. J. G. Qian, Q. Gao, J. F. Xue, H. W. Chen and M. S. Huang, Soil and ribbed concrete slab interface modeling using large shear box and 3D FEM, *Geomech. Eng.* **12**(2) (2017) 295–312.
19. C. F. Zhao, Y. Wu, C. Zhao and G. X. Tao, Experimental research on the clay-concrete interface shear behaviors considering the roughness and unloading effect, in *Proceedings of Geoshanghai International Conference*: *Fundamentals of Soil Behaviours* (2018), pp. 522–530.
20. M. Y. Zhang, S. K. Sang, Y. H. Wang and X. Y. Bai, Factors influencing the mechanical characteristics of a pile–soil interface in clay soil, *Front. Earth Sci.* **7** (2020) 11.
21. L. J. Su, W. H. Zhou, W. B. Chen and X. X. Jie, Effects of relative roughness and mean particle size

on the shear strength of sand-steel interface, *Meas.* **122** (2018) 339–346.
22. F. Han, E. Ganju, R. Salgado and M. Prezzi, Effects of interface roughness, particle geometry, and gradation on the sand-steel interface friction angle, *J. Geotech. Geoenviron. Eng.* **144**(12) (2018) 12.
23. M. Sharma, M. Samanta and S. Sarkar, A study on interface shear behavior of soil nails from pullout and direct shear tests, *Int. J. Phys. Model. Geotech.* **20**(1) (2020) 24–37.
24. P. Santos and E. N. B. S. Júlio, A state-of-art review on roughness quantification methods for concrete surfaces, *Constr. Build. Mater.* **38**(1) (2013) 912–923.
25. L. Millman and J. Giancaspro, Three-dimensional optical profilometry analysis of the international concrete repair institute concrete surface profiles (CSPs), *ACI Mater. J.* **110** (2013) 519–527.
26. B. Sengoz, A. Topal and S. Tanyel, Comparison of pavement surface texture determination by sand patch test and 3D laser scanning, *Period. Polytech.*, *Civ. Eng.* **45** (2012) 73–78.
27. L. Courard and M. Nelis, Surface analysis of mineral substrates for repair works: Roughness evaluation by profilometry and surfometry analysis, *Mag. Concr. Res.* **55**(4) (2003) 355–366.
28. W. Zhang, B. Zhou, X. Gu and H. Dai, Probability distribution model for cross-sectional area of corroded reinforcing steel bars, *J. Mater. Civ. Eng.* **26**(5) (2013) 822–832.
29. M. K. Kim, H. Sohn and C. C. Chang, Active dimensional quality assessment of precast concrete using 3D laser scanning, *Comput. Civ. Eng.* (2014) 622–628.
30. Y. Yoshimi and T. Kishida, A ring torsion apparatus for evaluating friction between soil and metal surfaces, *Geotech. Test. J.* **4**(4) (1981) 145–152.
31. L. Borana, J.-H. Yin, D. Singh and S. Shukla, Influence of matric suction and counterface roughness on shearing behavior of completely decomposed granitic soil and steel interface, *Indian Geotech. J.* **47** (2016).
32. Y. D. Xu and C. X. Qian, Fractal characterization of corroded surface profile in reinforcing steel bars, *Adv. Mater. Res.* **163–167** (2011) 3118–3121.
33. N. Lin, J. Guo, F. Xie, J. Zou, W. Tian, X. Yao, H. Zhang and B. Tang, Comparison of surface fractal dimensions of chromizing coating and P110 steel for corrosion resistance estimation, *Appl. Surf. Sci.* **311** (2014) 330–338.
34. C. Liang and W. Zhang, Fractal characteristic of pits distribution on 304 stainless steel corroded surface and its application in corrosion diagnosis, *J. Wuhan Univ. Technol., Mater. Sci. Ed.* **22**(3) (2007) 389–393.
35. X. Chen, J. Zhou and N. Ding, Fractal characterization of pore system evolution in cementitious materials, *KSCE J. Mater. Civ. Eng.* **19**(3) (2015) 719–724.
36. H. Xie, J. Wang and W. Xie, Fractal effects of surface roughness on the mechanical behavior of rock joints, *Chaos Soliton Fractals* **8**(2) (1997) 221–252.
37. H. Zhou and H. Xie, Direct estimation of the fractal dimensions of a fracture surface of rock, *Surf. Rev. Lett.* **10**(5) (2003) 751–762.
38. B. Huber, H. Hilbig, J. E. Drewes and E. Müller, Evaluation of concrete corrosion after short-and long-term exposure to chemically and microbially generated sulfuric acid, *Cem. Concr. Res.* **94** (2017) 36–48.
39. J. Xiao, W. Qu, W. Li and P. Zhu, Investigation on effect of aggregate on three non-destructive testing properties of concrete subjected to sulfuric acid attack, *Constr. Build. Mater.* **115** (2016) 486–495.
40. M. Mahdikhani, O. Bamshad and M. F. Shirvani, Mechanical properties and durability of concrete specimens containing nano silica in sulfuric acid rain condition, *Constr. Build. Mater.* **167** (2018) 929–935.
41. Z. T. Chang, X. J. Song, R. Munn and M. Marosszeky, Using limestone aggregates and different cements for enhancing resistance of concrete to sulphuric acid attack, *Cem. Concr. Res.* **35**(8) (2005) 1486–1494.
42. Y. Fan, Z. Hu, Y. Zhang and J. Liu, Deterioration of compressive property of concrete under simulated acid rain environment, *Constr. Build. Mater.* **24**(10) (2010) 1975–1983.
43. S. Xie, L. Qi and D. Zhou, Investigation of the effects of acid rain on the deterioration of cement concrete using accelerated tests established in laboratory, *Atmos. Environ.* **38**(27) (2004) 4457–4466.
44. A. P. Chandra and A. R. Gerson, The mechanisms of pyrite oxidation and leaching: A fundamental perspective, *Surf. Sci. Rep.* **65**(9) (2010) 293–315.
45. X. Li, X. Lin, K. Lin and T. Ji, Study on the degradation mechanism of sulphoaluminate cement sea sand concrete eroded by biological sulfuric acid, *Constr. Build. Mater.* **157** (2017) 331–336.
46. M. O'Connell, C. McNally and M. G. Richardson, Performance of concrete incorporating GGBS in aggressive wastewater environments, *Constr. Build. Mater.* **27**(1) (2012) 368–374.
47. M. S. Hasan, S. Setunge, D. W. Law and T. C. K. Molyneaux, Predicting life expectancy of concrete septic tanks exposed to sulfuric acid attack, *Mag. Concr. Res.* **65**(13) (2013) 793–801.
48. M. T. Bassuoni and M. L. Nehdi, Resistance of self-consolidating concrete to sulfuric acid attack with consecutive pH reduction, *Cem. Concr. Res.* **37**(7) (2007) 1070–1084.

49. Q. Zhou, J. Hill, E. A. Byars, J. C. Cripps, C. J. Lynsdale and J. H. Sharp, The role of pH in thaumasite sulfate attack, *Cem. Concr. Res.* **36**(1) (2006) 160–170.
50. R. Brueckner, S. J. Williamson and L. A. Clark, The effects of the thaumasite form of sulfate attack on skin friction at the concrete/clay interface, *Cem. Concr. Res.* **42**(2) (2012) 424–430.
51. M. B. Yao and J. P. Li, Effect of the degradation of concrete friction piles exposed to external sulfate attack on the pile bearing capacity, *Ocean Eng.* **173** (2019) 599–607.
52. L. Balachowski, Scale effect in shaft friction from the direct shear interface tests, *Arch. Civ. Mech. Eng.* **6** (2006) 13–28.
53. M. Mahmoodian and A. M. Alani, Effect of temperature and acidity of sulfuric acid on concrete properties, *J. Mater. Civ. Eng.* **29**(10) (2017) 04017154.
54. Z. Z. Yin, H. Zhu and G. H. Xu, A study of deformation in the interface between soil and concrete, *Comput. Geotech.* **17**(1) (1995) 75–92.
55. Z. H. Zhao, X. Z. Lv, W. M. Wang and Y. L. Tan, Damage evolution of bi-body model composed of weakly cemented soft rock and coal considering different interface effect, *SpringerPlus.* **5** (2016) 19.
56. F. D. Patton, Multiple modes of shear failure in rock, in *Proceedings of International Congress* (1966), pp. 509–513.
57. M. Colio Gutiérrez, Shear resistance for concrete dams: Laboratory tests (2013).